Report

Current Biology

ppGpp is a bacterial cell size regulator

Graphical abstract

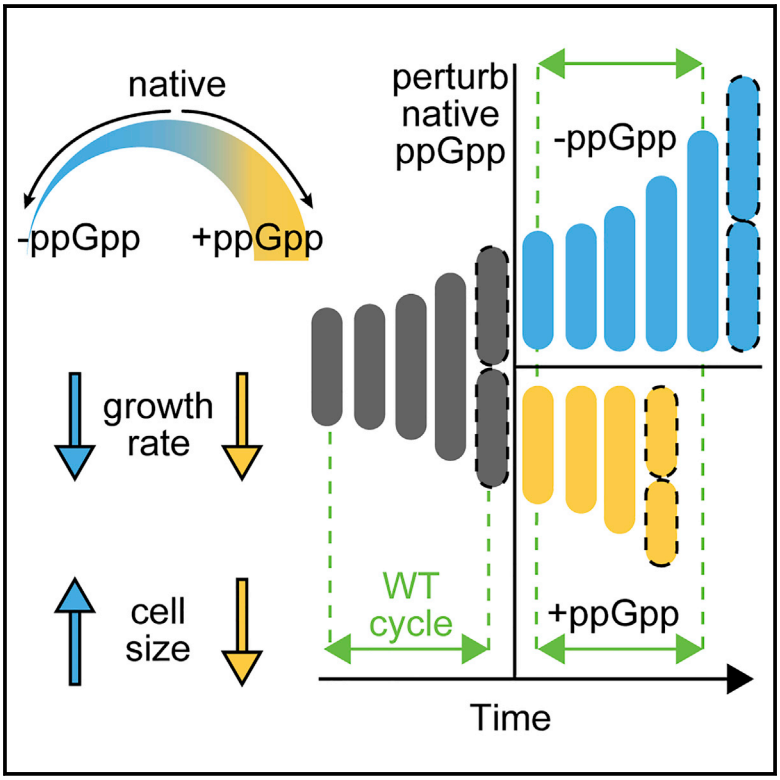

Authors

Ferhat Büke, Jacopo Grilli, Marco Cosentino Lagomarsino, Gregory Bokinsky, Sander J. Tans

Correspondence

tans@amolf.nl (S.J.T.), g.e.bokinsky@tudelft.nl (G.B.)

In brief

Working in *Escherichia coli,* Büke et al. discover that ppGpp is a cell division regulator that links growth rate with cell size.

Highlights

- ppGpp was directly tuned outside of native concentrations with a synthetic system
- Cell size inversely correlates with ppGpp concentration, not with growth rate
- ppGpp shifts can change cell division timing within a single cell cycle
- ppGpp can regulate cell size directly—not by modulating the growth rate

Büke et al., 2022, Current Biology *32*, 870–877
February 28, 2022
https://doi.org/10.1016/j.cub.2021.12.033

CellPress

CellPress

Current Biology

Report

ppGpp is a bacterial cell size regulator

Ferhat Büke,[1,2] Jacopo Grilli,[3] Marco Cosentino Lagomarsino,[4,5] Gregory Bokinsky,[1,6,*] and Sander J. Tans[1,2,6,7,8,*]
[1]Department of Bionanoscience, Kavli Institute of Nanoscience, Delft University of Technology, Delft, the Netherlands
[2]AMOLF, Amsterdam, the Netherlands
[3]The Abdus Salam International Centre for Theoretical Physics (ICTP), Strada Costiera 11, 34014 Trieste, Italy
[4]IFOM, FIRC Institute of Molecular Oncology, Via Adamello 16, 20143, Milan, Italy
[5]Physics Department, University of Milan, and I.N.F.N., Via Celoria 16, 20133, Milan, Italy
[6]These authors contributed equally
[7]Twitter: @sandertanslab
[8]Lead contact
*Correspondence: tans@amolf.nl (S.J.T.), g.e.bokinsky@tudelft.nl (G.B.)
https://doi.org/10.1016/j.cub.2021.12.033

SUMMARY

Growth and division are central to cell size. Bacteria achieve size homeostasis by dividing when growth has added a constant size since birth, termed the adder principle, by unknown mechanisms.[1,2] Growth is well known to be regulated by guanosine tetraphosphate (ppGpp), which controls diverse processes from ribosome production to metabolic enzyme activity and replication initiation and whose absence or excess can induce stress, filamentation, and small growth-arrested cells.[3–6] These observations raise unresolved questions about the relation between ppGpp and size homeostasis mechanisms during normal exponential growth. Here, to untangle effects of ppGpp and nutrients, we gained control of cellular ppGpp by inducing the synthesis and hydrolysis enzymes RelA and Mesh1. We found that ppGpp not only exerts control over the growth rate but also over cell division and thus the steady state cell size. In response to changes in ppGpp level, the added size already establishes its new constant value while the growth rate still adjusts, aided by accelerated or delayed divisions. Moreover, the magnitude of the added size and resulting steady-state birth size correlate consistently with the ppGpp level, rather than with the growth rate, which results in cells of different size that grow equally fast. Our findings suggest that ppGpp serves as a key regulator that coordinates cell size and growth control.

RESULTS

Bacterial cell size and growth coordination

Many bacterial species are known to display faster average growth and larger cell sizes in nutrient-rich media—a correlation that is also referred to as the growth law.[7–9] Yet, how cells coordinate size and growth is understood only partially. During the cell cycle, individual cells are found to grow until a constant volume is added on average and then divide. This adder principle is observed across diverse domains of life and can explain how the mean cell size remains constant in fixed conditions—despite random variations in cellular size at birth and the stochastic and exponential nature of growth.[1,2,10] While the molecular basis remains unresolved, mechanisms for the adder behavior have been proposed that are based on DNA replication initiation,[11–14] replication initiation and cell division,[15] cellular surface to volume ratio,[16] and the accumulation of division proteins.[17] In *Escherichia coli*, the signaling molecule guanosine tetraphosphate (ppGpp) is well known to be a key regulator of cellular growth.[18] The ppGpp concentration is inversely proportional to the exponential growth rate and accumulates to extreme levels during amino acid deprivation (a phenomenon specifically known as the stringent response) as well as during many other stress conditions.[6,19–24] ppGpp regulates the transcription of ribosomal RNA as well as other genes and is reported to allosterically control metabolic enzymes[25,26] and chromosome replication initiation.[27] However, despite the importance of growth in cellular size control, the role of ppGpp in size regulation mechanisms including the adder principle remains poorly understood.

Control of ppGpp synthesis and hydrolysis

To study the relation between ppGpp and cell growth and division and to disentangle it from metabolic limitation effects, two enzymes were used: the catalytic domain of the *E. coli* (p)ppGpp synthesis enzyme RelA (known as RelA')[6,28,29] fused to YFP, creating RelA'-YFP (here referred to as RelA*), and the *Drosophila melanogaster* ppGpp hydrolysis enzyme Mesh1[30,31] fused to CFP (fusion here referred to as Mesh1*), inducible by dox and IPTG, respectively (Figure 1A). As pppGpp produced by RelA* is rapidly dephosphorylated to form ppGpp, we refer to ppGpp for simplicity. Consistent with the opposing activities of RelA* and Mesh1*, the influence of either enzyme on exponential growth rate could be countered by the other in various growth media (Figures S1A and S1B). Therefore, balanced ppGpp synthesis and hydrolysis yielded the stable ppGpp levels that allow for normal exponential growth of homogeneous cell populations (Figure S1C). A number of experiments were consistent. First, expression of the fluorescent proteins alone did not affect cell

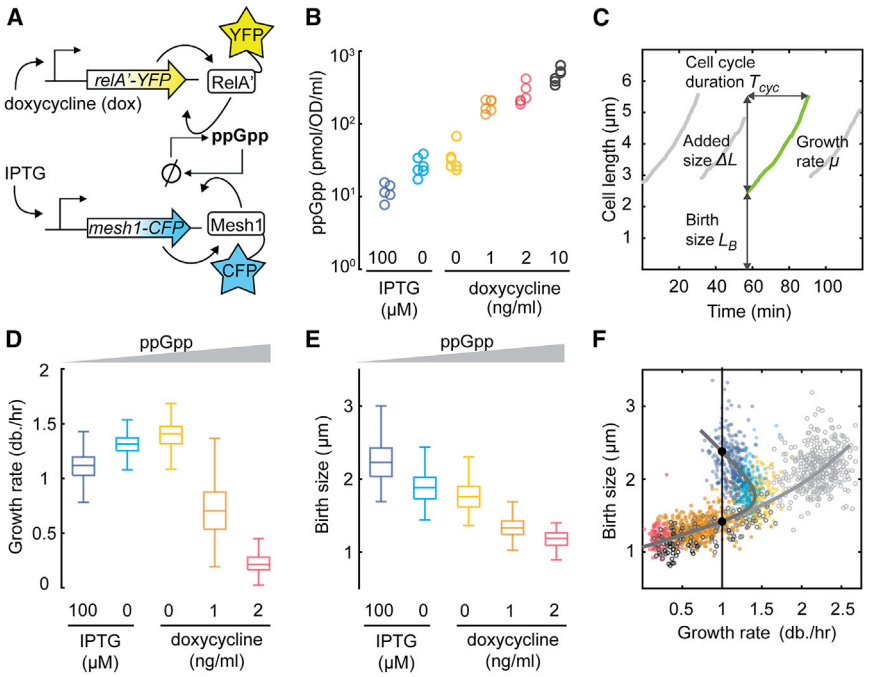

Figure 1. ppGpp exerts cell size control

(A) Scheme to control the ppGpp concentration. *E. coli* RelA truncate (*relA'*), fused to YFP, is induced by dox, which leads to ppGpp via synthesis and dephosphorylation of pppGpp (not shown). The ppGpp hydrolysis enzyme Mesh1, fused to CFP, is induced by IPTG.

(B) Intracellular ppGpp concentrations after induction of *mesh1-CFP* (*mesh1** from here) or *relA'-YFP* (*relA** from here) compared to basal levels, in glucose minimal medium. Shown are two to three measurements from two biological replicates.

(C) Measured cell length for a single lineage, as grown in a microfluidic device. For each cell cycle we quantified size (length) at birth (L_B), cell cycle duration (T_{cyc}), added size (ΔL), and the growth rate (μ) by exponential fitting.

(D) Growth rate for increasing ppGpp levels in glucose minimal medium (left to right, see [B]). Left to right: N = 270, 254, 255, 479, 119 cell cycles. μ peaks at basal ppGpp levels (no induction) and then decreases.

(E) Birth size for increasing ppGpp levels. Conditions as in (B). L_B increases continuously, while μ decreases for below-basal ppGpp levels.

(F) Birth length against growth rate. Closed circles: single cell cycles in minimal media, colors and conditions as in (B). Drawn curves are guides to the eye. Notably, for below-basal ppGpp, slower growing cells are larger, owing to an inversion of the growth law. Cells of different size can thus have the same growth rate (black dots). Open circles: single cell cycles in glucose rich media including amino acids, with 2 ng/mL, 1 ng/mL, or 0 ng/mL dox, and N = 70, 68, 340 cell cycles (dark to light gray).

See Figure S1 for further characterization of the plasmids.

size or growth rate (Figures S1D–S1G). Second, a strain unable to produce ppGpp (ppGpp^0 or *ΔrelA, ΔspoT*) did not grow in various minimal media lacking amino acids unless *relA** and *mesh1** were induced in a balanced manner (Figure S1B),[6,30] in line with ppGpp activating amino acid biosynthesis operons.[32,33] Third, in glucose-rich medium containing amino acids, when ppGpp must be very low, Mesh1* induction did not affect growth (Figure S1H). Finally, we quantified ppGpp in wild-type *E. coli* (*relA+ spoT+*). These data confirmed that ppGpp levels indeed varied above and below normal concentrations when inducing *relA** or *mesh1**, respectively (Figure 1B).

ppGpp exerts cell size control

We studied the effects of ppGpp manipulation at the single-cell level using a microfluidic device that allowed media exchange, phase contrast, fluorescence microscopy, and cell-tracking algorithms.[10,34] We determined the length at birth (L_B) and division (L_D), the cycle duration (T_{cyc}), and exponential growth or elongation rate (μ) for each cell cycle and RelA* and Mesh1* enzyme concentrations, as quantified by the mean fluorescence per pixel (Figure 1C; Figure S1C). We expressed either RelA* or Mesh1* at moderate levels in the wild-type background to produce deviations in ppGpp relative to basal levels while maintaining balanced exponential growth (Figures 1D–1F).

As ppGpp decreased from above to below basal levels in glucose minimal medium, the (population-mean) trend in μ showed an optimum while L_B increased monotonically (Figures 1D and 1E). The relation between L_B and μ (Figure 1F) contained a number of intriguing features. First, as ppGpp decreased, both L_B and μ increased initially, in agreement with the well-known finding that faster-growing cells are larger. However, decreasing ppGpp further led to an inverted trend, in which slower growing cells are larger. This deviation began at near-endogenous ppGpp levels. A counterintuitive consequence of this inversion is that excursions above and below this endogenous ppGpp level lead to cells that differ in size but grow equally fast (Figure 1F, two example black dots on vertical line). The same trends were observed for the ppGpp^0 strain with RelA* and Mesh1* expression (Figure S2A).

The data are thus inconsistent with models in which ppGpp affects cell size by controlling growth. In such *hierarchical* models, L_B would follow the increase-optimum-decrease trend observed for μ (Figure 1D). Instead, the monotonic increase of L_B with increasing ppGpp (Figure 1E) suggested that ppGpp affects L_B in a way that is not mediated *via* μ. If ppGpp indeed modulates the size of cells in this manner, we surmised it should play a role in the adder mechanism, which maintains the cell size constant against stochastic variations in birth size.

ppGpp dynamically controls added cell size

In order to investigate the effect of ppGpp on the added size, we quantified the added length (ΔL) each cell cycle. First, we found that the adder principle was obeyed at all ppGpp concentrations: for the different levels of dox and IPTG induction, ΔL was birth-size independent (Figure 2A). In line with previous adder principle observations, we find that T_{cyc} rather than μ is modulated to achieve a constant ΔL, as larger-born cells divide sooner (Figure 2B). Indeed, ΔL increased monotonically with decreasing ppGpp (Figure S2B) and thus did not follow the trend observed for μ (Figure 1D). These data indicated that the added size

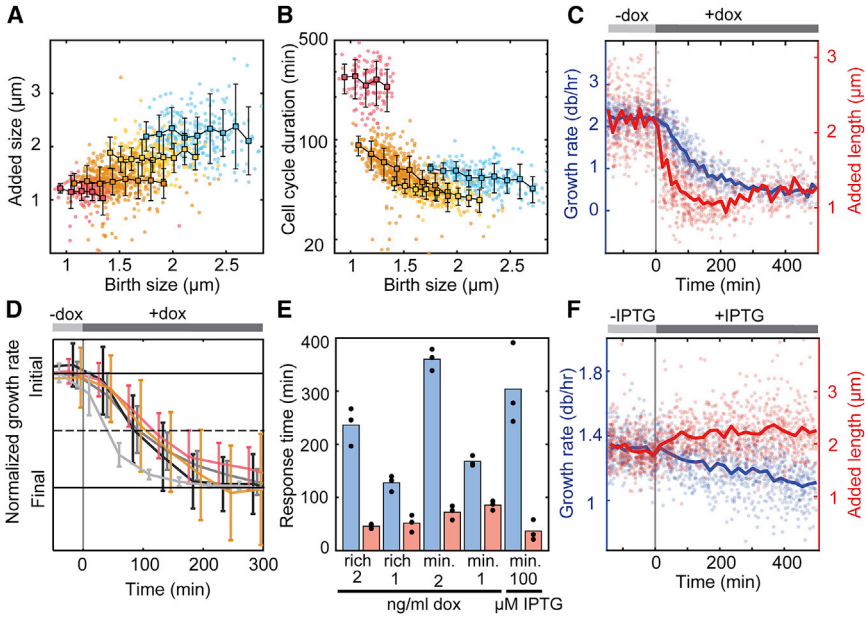

Figure 2. ppGpp dynamically controls added cell size

(A) Cell length added per cell cycle (ΔL) against birth length (L_B) of that cycle, for different constant ppGpp levels. Dots are single cell cycles, squares are means for L_B bin, bars are SE. Left to right: clouds for decreasing ppGpp levels, starting with dox in ng/mL: 2 (red), 1 (orange), 0 (yellow), and 100 μM IPTG (blue). N = 119, 479, 255, 270 cell cycles. For each cloud, ΔL is constant for different L_B, consistent with the adder principle.

(B) Cell cycle duration (T_{cyc}) against birth length (L_B) of that cycle. Within a cloud, when L_B is smaller T_{cyc} is typically larger on average, indicating it is modulated as cells compensate for stochastic variations in L_B, which is consistent with the adder principle. Colors and conditions as in (A).

(C) Growth rate (μ) and added size (ΔL) during a ppGpp increase. Circles are single cell cycles, lines are moving averages, for a shift from 0 to 2 ng/mL dox, in rich glucose medium. ΔL responds faster than μ and reaches the post-shift value while μ decreases.

(D) Growth rate (μ) during different ppGpp increases (*relA** induction for different dox concentrations), in glucose rich and minimal media. μ response timescale for these various conditions is assessed by normalizing rate to initial (pre-shift) and final (post-shift) value. Top bar indicates dox induction. In minimal media, shift from 0 ng/mL dox to: 2 (pink), and 1 (orange). In rich media, shift from 0 ng/mL dox to: 1 (dark gray), 2 (intermediate gray), and 10 (light gray). Bars are SEM. For moderate (1 and 2 ng/mL) shifts, the adaptation time is similar and growth remains exponential. For the larger 10 ng/mL shift, the growth decreases faster and arrests after the shift, in line with ppGpp approaching stringent response levels.

(E) Response time for μ (blue) and ΔL (red) (see STAR Methods). Black dots represent one third of the data points. ΔL responds faster than μ under all moderate shifts.

(F) Growth (μ) and added size (ΔL) during a ppGpp decrease. Circles are single cell cycles, lines are moving averages, for shift from 0 to 100 μM IPTG, in glucose minimal medium. For the resulting below-basal ppGpp levels, the added cell size increases while growth rate decreases.

See Figure S2 for parallel results in the ppGpp^0 strain and the effects of ppGpp shifts on other parameters.

correlated with population-average ppGpp concentration rather than the rate of growth.

Next, we considered how shifts in ppGpp concentration affect cell size and its control dynamically. Within the microfluidic flow-cell, we followed individual cells as they were exposed to a shift from basal ppGpp concentrations to different levels of *relA** induction in various growth media. First, the growth response underscored the important differences between moderate *relA** induction, focused on here (1 and 2 ng/mL dox), and strong induction (10 ng/mL dox) that raises ppGpp to near-stringent response concentrations.[35] The former allows continued exponential growth (Figures 2C and 2D) while we find that the latter rapidly reduces μ and eventually arrests growth.

Notably, however, the added size responded more rapidly than the growth rate, even for low *relA** induction levels. ΔL decreased halfway at about 25 min and reached its final value at about 55 min (Figure 2C, red trace), while μ decreased halfway at about 100 min and attained its final value at about 300 min (Figure 2C, blue trace). A similar pattern of rapid ΔL and slow μ responses were observed for different media and dox induction levels (Figure 2E), as well as for *mesh1** induction (Figure 2F). Consistently, ΔL increased more rapidly than μ decreased upon *mesh1** induction (Figure 2F). Upon *relA** or *mesh1** induction, the cell width also decreased and increased, respectively, albeit more slowly than for the added length (Figure S2C). We note that after reaching the final value, we found that ΔL can show an additional low-amplitude response component that is slower, in the form of a small undershoot and recovery after first reaching the final value at about 55 min (Figure 2C). This slower variation was not seen in the majority of the conditions (Figure S3A). It suggested a fine-grained adaptation of the system and may reflect an equilibration of other cellular processes in response to the ppGpp change that in turn affect ΔL.

The data show a temporal order in which ΔL responds to ppGpp deviations prior to μ. Indeed, ΔL typically has already reached its post-shift level when μ has decreased only halfway from pre-induction to post-induction level (Figures 2D–2F). These data support the idea that the effect of ppGpp on ΔL is not mediated by μ. We hypothesize that a change in ppGpp concentration sets a new added size by affecting the division frequency, which in turn results in a new steady-state birth size. Note that these observations do not imply that ppGpp control over size and growth are uncoupled. In addition to the effects observed here, there can be other processes that affect both the growth rate and division, including transcriptional control, altered metabolic conditions, stress or DNA damage.

Division accelerates transiently to achieve constant added size

We used mathematical modeling to understand the interplay between growth, division, and size and compare different possible scenarios. Current size homeostasis models consider constant growth conditions, as well as a strict coupling between μ and ΔL.[1,2,36,37] We first tested a hierarchical model (Figure 3A), which

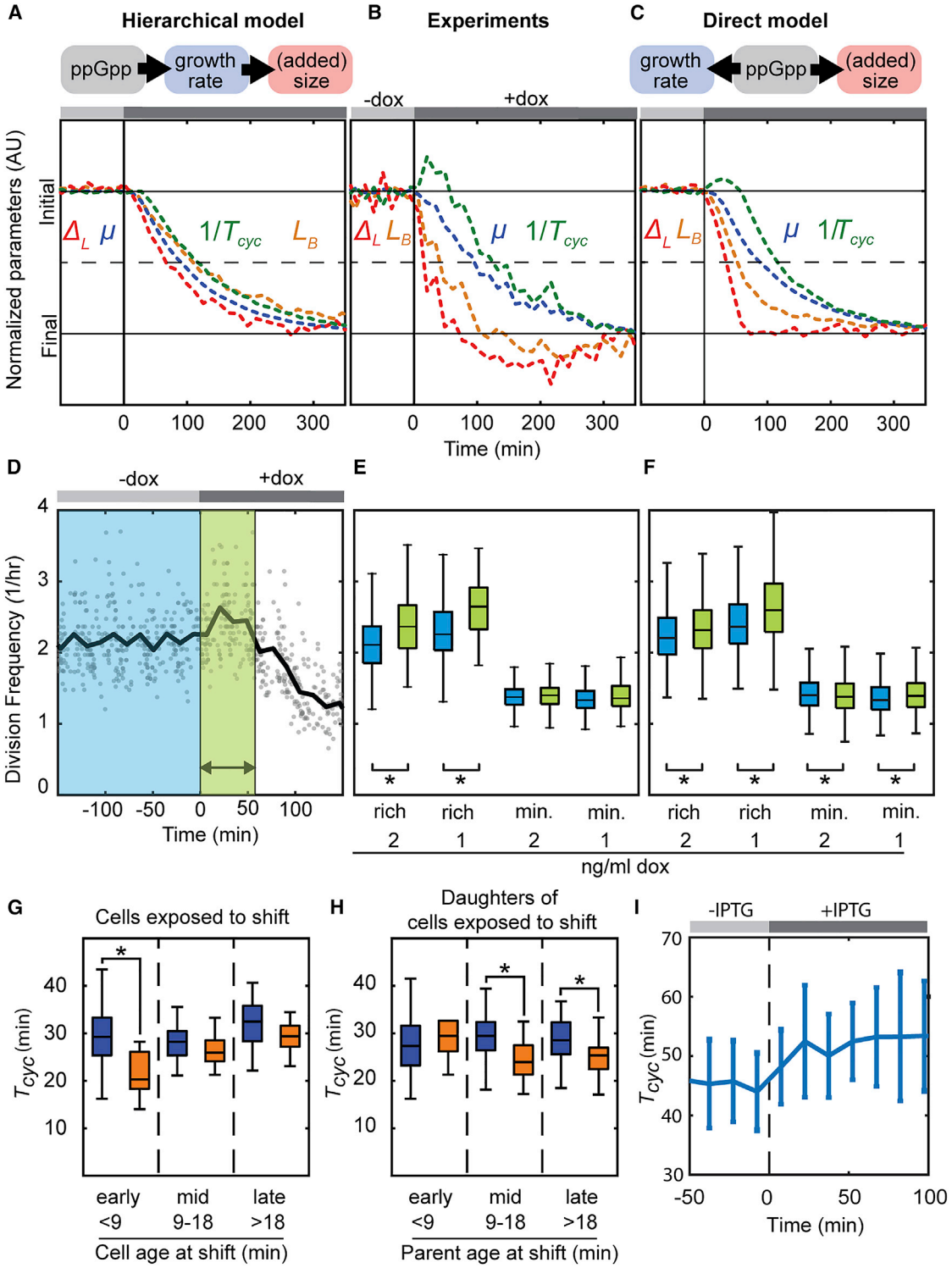

Figure 3. Division accelerates transiently to achieve constant added size

(A) Predictions of hierarchical model, in which ppGpp affects the growth rate (μ) and in turn added size adjusts to the growth rate. To compare response speeds, indicated quantities are normalized to initial (pre-shift) and final (post-shift) values. Top bar indicates ppGpp increase. See Methods S1 for a detailed description of the modeling framework used.

(B) Experimental data. Conditions as in (A).

(legend continued on next page)

thus preserves the μ-ΔL coupling as growth conditions change. This model takes the observed initial and final values of μ and ΔL as input, lets μ decrease exponentially with the observed rate, and averages over multiple resulting simulated stochastic trajectories in ΔL and division frequency $1/T_{cyc}$. Note that while $1/T_{cyc}$ equals μ for exponentially growing populations in constant conditions, these quantities may not be strictly coupled when conditions change. The results of the hierarchical model (Figure 3A) appeared inconsistent with the experimental observations (Figure 3B). In particular, ΔL and μ decrease at similar rates and L_B decreases slower than μ in this model (Figure 3A), but the experiments show that both ΔL and L_B decrease faster than μ (Figure 3B). Notably, the experimental data also indicate a transient increase in the division frequency $1/T_{cyc}$ before it decreases (Figure 3B), unlike the hierarchical control model (Figure 3A).

Next, we considered a model of *direct* ppGpp control, in which ppGpp changes also affect ΔL but not via changes in μ (Figure 3C). In this model, as also observed in the data (Figure 2C), the mean ΔL responds directly by decreasing linearly to its post-shift value in about two pre-shift cell-cycles (note that division events in the averaged lineages are not synchronized), while μ decreases in the same way as in the previous model (Figure S3A). The direct control model reproduces many features of the experimental data. Specifically, L_B responds slower than ΔL but faster than μ, and $1/T_{cyc}$ showed a transient increase (Figures 3B–3F).

This increase in $1/T_{cyc}$ may appear paradoxical, as it must decrease ultimately to match the lower μ. However, with μ remaining comparatively high upon the shift and ΔL decreasing faster, it is logical that divisions occur earlier as well. Nonetheless, the up and down modulation of the division frequency is notable. Together, these findings support the notion that the cells establish new targets for ΔL and L_B that are not set by the growth rate and thus produce a transiently varying division frequency. Further observations are consistent with the direct model (Figures 3D–3H). First, $1/T_{cyc}$ changes on a timescale that is shorter than both the cell cycle duration (28 min) and the C+D period (∼65–75 min).[38] When ppGpp shifts early in the cycle, the duration of that same cycle is reduced from 28 to 22 min (Figure 3G, $p < 10^{-3}$). Divisions occurred down to 15 min after the shift, which provides a lower estimate of the response time. For shifts occurring mid-cycle or late, it is logically the next (daughter) cycle that is reduced (Figure 3H, $p < 10^{-3}$). Thus, division can respond to ppGpp shifts within one cell cycle and depends on the timing of this shift within the cycle. Second, the direct model predicts that in minimal media, the $1/T_{cyc}$ changes would be much smaller compared to rich media and indeed may be too small to detect (Figure 3F), owing to the lower μ. Third, upon Mesh1* induction, T_{cyc} increases within 25 min and then stays constant (Figure 3I). These results indicate that ppGpp can exert control over division, and thus over cell size, in a way that is not mediated hierarchically through its effects on DNA replication initiation and the rate of growth. Experiments using a natural trigger of ppGpp synthesis supports this finding. Rapid amino acid starvation, which activates ppGpp synthesis by RelA in wild-type cells, led to multiple divisions and a population of small cells within 2 h. In contrast, Δ*relA* cells divided at most once after the downshift and remained at a size similar to the pre-downshift average (Figure S3B).

DISCUSSION

Elucidating the coordination between cell growth and cell cycle progression is a foundational challenge of microbial physiology. By directly manipulating ppGpp, we found that ppGpp is a cell division regulator and therefore serves as a link between growth and size control mechanisms. More specifically, we showed that *E. coli* cells do not follow a hierarchical model, in which cell size adjusts to the growth rate (as in the general growth law[7,8,13,39]) and ppGpp controls growth (by tuning ribosome production depending on amino acid availability, for instance). Rather, the (added) size correlates with the level of ppGpp (instead of the growth rate) and adjusts rapidly to ppGpp deviations, prior to the growth rate response. These observations indicate that ppGpp exerts control over cell division in a way that is not mediated by the growth rate.

The findings lead to a number of speculations and implications. ppGpp is known to reflect diverse signals, including nutritional conditions, stress, biosynthetic activity, and metabolite availability.[40,41] The proposed mechanism thus allows division control to integrate a wide spectrum of relevant growth factors. It may also help to accommodate physiological limitations. For instance, ribosome excess may require larger cells but can incur a growth penalty due to metabolic costs, while the monotonic

(C) Predictions of direct model, in which ppGpp exerts control over division and hence (added) size, without being mediated by μ. Conditions as in (A). The data agree with direct model, both in terms of the temporal order of the responses and the transient acceleration of divisions. See Figure S3A for a comparison of both models against experiments.

(D) Quantification of transient effects in the division frequency ($1/T_{cyc}$). Data are averaged in purple and green (width equals $2*T_{cyc}$, black arrow) zones to produce data in (E) and (F). Circles are single cell cycles for shift from 0 to 2 ng/mL dox, in glucose minimal medium. Drawn line is moving average.

(E) Experimental pre- and post-shift division frequency ($1/T_{cyc}$), as defined in (D). In rich media, up to a ∼15% increase is observed between. Star: $p < 0.01$. (N = 340, 187, 98, 62, 255, 193, 226, 220 left to right).

(F) Direct model yields transient changes for 1/Tcyc. Star: $p < 0.01$. Note the model detects small changes due to high number of cells used (5,000 pre-shift, 3,000 post-shift).

(G) Measured cell cycle duration (T_{cyc}) during ppGpp up shift (2 ng/mL dox, rich media, orange) compared to cells before the shift (between −140 and −90 min., blue). Cells that are young (<9 min. after birth) during shift show decreased T_{cyc} in the same cycle as the shift. N = 61, 11, 28, 23, 51, 33. Star: $p < 10^{-3}$. See Figure S3B.

(H) T_{cyc} of the progeny of the cells in (G) (orange), showing decreases when the ppGpp shift occurs mid-cycle and late in their parent. N = 73, 6, 22, 25, 48, 43. Star and blue boxplots as in (G).

(I) Cell cycle duration during ppGpp down-shift. Induction of *mesh1** (T = 0 min) leads to increase in T_{cyc} within one cell cycle, suggesting inhibition of division by decreased ppGpp levels. Note a slight increase in RNA content is observed in cells experiencing a ppGpp downshift in minimal medium (Figure S3C).
See Figure S3.

size-growth relation of hierarchical models would impose smaller cells at lower growth. We indeed found that Mesh1* induction not only reduced growth (Figure 1D) but also increased ribosome levels (Figure S3C),[30] which helps to explain the monotonicity deviation (Figure 1F). These considerations are consistent with the idea that *E. coli* maximizes its growth rate rather than its size, and thus that size is modulated to accommodate associated requirements. Bacteria may deviate from the size-growth monotonicity also in other situations, with possible roles for ppGpp. Translation inhibitors can depress ppGpp and increase cell size,[13,42] and overexpression of non-functional proteins can yield larger cells,[43] while stochasticity can also cause monotonicity deviations (Figure S2A). Our results further indicate that ppGpp may serve to control recently observed division delays during nutrient up-shifts.[44]

The growth changes observed here were slow compared to those triggered by ppGpp concentrations reached during the stringent response. Note that ppGpp increases can result in physiological effects that are slower than the immediate effects on its direct targets, such as RNA polymerases. For instance, ppGpp control of rRNA production can lead to lower ribosome levels by growth-mediated dilution on generation timescales. We found that division can respond within 20 min, which may reflect the time required to express divisome components or to complete processes such as chromosome segregation and division ring assembly, which are regulated by nucleoid occlusion, the Min system, and other mechanisms.[34,45]

Diverse mechanisms have been proposed to explain cell size homeostasis and its dependence on growth.[11–17] Our findings suggest these mechanisms are under the control of ppGpp. For instance, the constant added size is proposed to result from the accumulation of a signaling molecule throughout the cell cycle, which triggers division when a threshold is exceeded.[17] One may speculate that ppGpp alters the production of this molecule and its threshold. Owing to the central role of ppGpp in metabolism and its many regulatory targets (hundreds of genes[46] and dozens of proteins[26,47,48]), ppGpp could control size in many possible ways. This may occur by transcriptional or post-transcriptional regulation, for instance of divisome proteins. It was found that OpgH can suppress FtsZ ring formation depending on the growth rate.[49] One may consider whether OpgH mediates the ppGpp division effects, though it is not a known ppGpp interactor.[26,47,48] Nucleoid occlusion mechanisms have also been proposed to be involved in cell size regulation.[1,50] Nucleoid volume could be modulated by ppGpp-induced decrease in the overall DNA replication initiation[27,51] or transcription rates.[52,53]

In conclusion, our findings establish a link between ppGpp, the central signaling molecule in bacterial growth, and cell size homeostasis, which has implications for the diverse cellular components and processes that are involved in these two pivotal cellular control mechanisms.

STAR★METHODS

Detailed methods are provided in the online version of this paper and include the following:

- KEY RESOURCES TABLE
- RESOURCE AVAILABILITY
  - Lead contact
  - Materials availability
  - Data and code availability
- EXPERIMENTAL MODEL AND SUBJECT DETAILS
  - Strains and plasmids
  - Culture conditions
- METHOD DETAILS
  - Sample collection and analysis for ppGpp, protein, and RNA quantification
  - Microfluidic flow cell
  - Imaging and image analysis
  - ppGpp quantification via LC/MS
- QUANTIFICATION AND STATISTICAL ANALYSIS
  - Calculation of response time
  - Division frequency analysis
  - Double normalization
  - Models

SUPPLEMENTAL INFORMATION

Supplemental information can be found online at https://doi.org/10.1016/j.cub.2021.12.033.

ACKNOWLEDGMENTS

We thank Mike Cashel for sharing *E. coli* CF10237 and CF12355. We thank Rebecca McKenzie, Martijn Wehrens, Nicole Imholz, and Marek Noga for experimental assistance and helpful discussions throughout the project, Daan J. Kiviet for sharing his mold for the microfluidic device, and Flora Yang for assistance with LCMS measurements. Work in the Tans and Bokinsky labs is supported by the Netherlands Organization for Scientific Research (NWO). F.B. was supported as part of the Frontiers of Nanoscience program.

AUTHOR CONTRIBUTIONS

G.B., S.J.T., and F.B. conceived the experiments, F.B. performed the experiments, F.B., M.C.L., and J.G. performed the modeling, all authors contributed to the writing of the manuscript.

DECLARATION OF INTERESTS

The authors declare no competing interests.

Received: June 4, 2020
Revised: August 27, 2021
Accepted: December 13, 2021
Published: January 5, 2022

REFERENCES

1. Campos, M., Surovtsev, I.V., Kato, S., Paintdakhi, A., Beltran, B., Ebmeier, S.E., and Jacobs-Wagner, C. (2014). A constant size extension drives bacterial cell size homeostasis. Cell *159*, 1433–1446.
2. Taheri-Araghi, S., Bradde, S., Sauls, J.T., Hill, N.S., Levin, P.A., Paulsson, J., Vergassola, M., and Jun, S. (2017). Cell-Size Control and Homeostasis in Bacteria. Curr. Biol. *27*, 1392.
3. Magnusson, L.U., Gummesson, B., Joksimović, P., Farewell, A., and Nyström, T. (2007). Identical, independent, and opposing roles of ppGpp and DksA in Escherichia coli. J. Bacteriol. *189*, 5193–5202.
4. Schreiber, G., Ron, E.Z., and Glaser, G. (1995). ppGpp-mediated regulation of DNA replication and cell division in Escherichia coli. Curr. Microbiol. *30*, 27–32.

5. Vadia, S., Tse, J.L., Lucena, R., Yang, Z., Kellogg, D.R., Wang, J.D., and Levin, P.A. (2017). Fatty Acid Availability Sets Cell Envelope Capacity and Dictates Microbial Cell Size. Curr. Biol. *27*, 1757–1767.
6. Xiao, H., Kalman, M., Ikehara, K., Zemel, S., Glaser, G., and Cashel, M. (1991). Residual guanosine 3¢,5¢-bispyrophosphate synthetic activity of relA null mutants can be eliminated by spoT null mutations. J. Biol. Chem. *266*, 5980–5990.
7. Pierucci, O. (1978). Dimensions of Escherichia coli at various growth rates: model for envelope growth. J. Bacteriol. *135*, 559–574.
8. Schaechter, M., Maaloe, O., and Kjeldgaard, N.O. (1958). Dependency on medium and temperature of cell size and chemical composition during balanced grown of Salmonella typhimurium. J. Gen. Microbiol. *19*, 592–606.
9. Vadia, S., and Levin, P.A. (2017). Bacterial Size: Can't Escape the Long Arm of the Law. Curr. Biol. *27*, R339–R341.
10. Kiviet, D.J., Nghe, P., Walker, N., Boulineau, S., Sunderlikova, V., and Tans, S.J. (2014). Stochasticity of metabolism and growth at the single-cell level. Nature *514*, 376–379.
11. Cooper, S., and Helmstetter, C.E. (1968). Chromosome replication and the division cycle of Escherichia coli B/r. J. Mol. Biol. *31*, 519–540.
12. Ho, P.Y., and Amir, A. (2015). Simultaneous regulation of cell size and chromosome replication in bacteria. Front. Microbiol. *6*, 662.
13. Si, F., Li, D., Cox, S.E., Sauls, J.T., Azizi, O., Sou, C., Schwartz, A.B., Erickstad, M.J., Jun, Y., Li, X., and Jun, S. (2017). Invariance of Initiation Mass and Predictability of Cell Size in Escherichia coli. Curr. Biol. *27*, 1278–1287.
14. Wallden, M., Fange, D., Lundius, E.G., Baltekin, Ö., and Elf, J. (2016). The Synchronization of Replication and Division Cycles in Individual E. coli Cells. Cell *166*, 729–739.
15. Witz, G., van Nimwegen, E., and Julou, T. (2019). Initiation of chromosome replication controls both division and replication cycles in *E. coli* through a double-adder mechanism. eLife *8*, e48063.
16. Harris, L.K., and Theriot, J.A. (2016). Relative Rates of Surface and Volume Synthesis Set Bacterial Cell Size. Cell *165*, 1479–1492.
17. Si, F., Le Treut, G., Sauls, J.T., Vadia, S., Levin, P.A., and Jun, S. (2019). Mechanistic Origin of Cell-Size Control and Homeostasis in Bacteria. Curr. Biol. *29*, 1760–1770.
18. Potrykus, K., Murphy, H., Philippe, N., and Cashel, M. (2011). ppGpp is the major source of growth rate control in E. coli. Environ. Microbiol. *13*, 563–575.
19. Cashel, M., and Gallant, J. (1969). Two compounds implicated in the function of the RC gene of Escherichia coli. Nature *221*, 838–841.
20. Ferullo, D.J., and Lovett, S.T. (2008). The stringent response and cell cycle arrest in Escherichia coli. PLoS Genet. *4*, e1000300.
21. Jishage, M., Kvint, K., Shingler, V., and Nyström, T. (2002). Regulation of sigma factor competition by the alarmone ppGpp. Genes Dev. *16*, 1260–1270.
22. Traxler, M.F., Summers, S.M., Nguyen, H.T., Zacharia, V.M., Hightower, G.A., Smith, J.T., and Conway, T. (2008). The global, ppGpp-mediated stringent response to amino acid starvation in Escherichia coli. Mol. Microbiol. *68*, 1128–1148.
23. Vinella, D., Albrecht, C., Cashel, M., and D'Ari, R. (2005). Iron limitation induces SpoT-dependent accumulation of ppGpp in Escherichia coli. Mol. Microbiol. *56*, 958–970.
24. Seyfzadeh, M., Keener, J., and Nomura, M. (1993). spoT-dependent accumulation of guanosine tetraphosphate in response to fatty acid starvation in Escherichia coli. Proc. Natl. Acad. Sci. USA *90*, 11004–11008.
25. Wang, B., Grant, R.A., and Laub, M.T. (2020). ppGpp Coordinates Nucleotide and Amino-Acid Synthesis in E. coli During Starvation. Mol. Cell *80*, 29–42.
26. Wang, B., Dai, P., Ding, D., Del Rosario, A., Grant, R.A., Pentelute, B.L., and Laub, M.T. (2019). Affinity-based capture and identification of protein effectors of the growth regulator ppGpp. Nat. Chem. Biol. *15*, 141–150.
27. Kraemer, J.A., Sanderlin, A.G., and Laub, M.T. (2019). The Stringent Response Inhibits DNA Replication Initiation in E. coli by Modulating Supercoiling of *oriC*. MBio *10*, e01330-19.
28. Schreiber, G., Metzger, S., Aizenman, E., Roza, S., Cashel, M., and Glaser, G. (1991). Overexpression of the relA gene in Escherichia coli. J. Biol. Chem. *266*, 3760–3767.
29. Gropp, M., Strausz, Y., Gross, M., and Glaser, G. (2001). Regulation of Escherichia coli RelA requires oligomerization of the C-terminal domain. J. Bacteriol. *183*, 570–579.
30. Zhu, M., and Dai, X. (2019). Growth suppression by altered (p)ppGpp levels results from non-optimal resource allocation in Escherichia coli. Nucleic Acids Res. *47*, 4684–4693.
31. Sun, D., Lee, G., Lee, J.H., Kim, H.Y., Rhee, H.W., Park, S.Y., Kim, K.J., Kim, Y., Kim, B.Y., Hong, J.I., et al. (2010). A metazoan ortholog of SpoT hydrolyzes ppGpp and functions in starvation responses. Nat. Struct. Mol. Biol. *17*, 1188–1194.
32. Paul, B.J., Berkmen, M.B., and Gourse, R.L. (2005). DksA potentiates direct activation of amino acid promoters by ppGpp. Proc. Natl. Acad. Sci. USA *102*, 7823–7828.
33. Paul, B.J., Barker, M.M., Ross, W., Schneider, D.A., Webb, C., Foster, J.W., and Gourse, R.L. (2004). DksA: a critical component of the transcription initiation machinery that potentiates the regulation of rRNA promoters by ppGpp and the initiating NTP. Cell *118*, 311–322.
34. Wehrens, M., Ershov, D., Rozendaal, R., Walker, N., Schultz, D., Kishony, R., Levin, P.A., and Tans, S.J. (2018). Size Laws and Division Ring Dynamics in Filamentous Escherichia coli cells. Curr. Biol. *28*, 972–979.
35. Noga, M.J., Büke, F., van den Broek, N.J.F., Imholz, N.C.E., Scherer, N., Yang, F., and Bokinsky, G. (2020). Posttranslational Control of PlsB Is Sufficient To Coordinate Membrane Synthesis with Growth in Escherichia coli. MBio *11*, e02703–e02719.
36. Osella, M., Nugent, E., and Cosentino Lagomarsino, M. (2014). Concerted control of Escherichia coli cell division. Proc. Natl. Acad. Sci. USA *111*, 3431–3435.
37. Ho, P.Y., Lin, J., and Amir, A. (2018). Modeling Cell Size Regulation: From Single-Cell-Level Statistics to Molecular Mechanisms and Population-Level Effects. Annu. Rev. Biophys. *47*, 251–271.
38. Bremer, H., and Dennis, P.P. (2008). Modulation of Chemical Composition and Other Parameters of the Cell at Different Exponential Growth Rates. Ecosal Plus *3*, https://doi.org/10.1128/ecosal.5.2.3.
39. Vadia, S., and Levin, P.A. (2015). Growth rate and cell size: a re-examination of the growth law. Curr. Opin. Microbiol. *24*, 96–103.
40. Hauryliuk, V., Atkinson, G.C., Murakami, K.S., Tenson, T., and Gerdes, K. (2015). Recent functional insights into the role of (p)ppGpp in bacterial physiology. Nat. Rev. Microbiol. *13*, 298–309.
41. Ronneau, S., and Hallez, R. (2019). Make and break the alarmone: regulation of (p)ppGpp synthetase/hydrolase enzymes in bacteria. FEMS Microbiol. Rev. *43*, 389–400.
42. Baracchini, E., and Bremer, H. (1988). Stringent and growth control of rRNA synthesis in Escherichia coli are both mediated by ppGpp. J. Biol. Chem. *263*, 2597–2602.
43. Basan, M., Zhu, M., Dai, X., Warren, M., Sévin, D., Wang, Y.P., and Hwa, T. (2015). Inflating bacterial cells by increased protein synthesis. Mol. Syst. Biol. *11*, 836.
44. Panlilio, M., Grilli, J., Tallarico, G., Iuliani, I., Sclavi, B., Cicuta, P., and Lagomarsino, M.C. (2020). Threshold accumulation of a constitutive protein explains E. coli cell division behavior in nutrient upshifts. bioRxiv. https://doi.org/10.1101/2020.08.03.233908.
45. Arjes, H.A., Kriel, A., Sorto, N.A., Shaw, J.T., Wang, J.D., and Levin, P.A. (2014). Failsafe mechanisms couple division and DNA replication in bacteria. Curr. Biol. *24*, 2149–2155.
46. Liu, K., Bittner, A.N., and Wang, J.D. (2015). Diversity in (p)ppGpp metabolism and effectors. Curr. Opin. Microbiol. *24*, 72–79.
47. Kanjee, U., Ogata, K., and Houry, W.A. (2012). Direct binding targets of the stringent response alarmone (p)ppGpp. Mol. Microbiol. *85*, 1029–1043.

48. Zhang, Y., Zborníková, E., Rejman, D., and Gerdes, K. (2018). Novel (p)ppGpp Binding and Metabolizing Proteins of *Escherichia coli*. MBio *9*, e02188-17.

49. Hill, N.S., Buske, P.J., Shi, Y., and Levin, P.A. (2013). A moonlighting enzyme links Escherichia coli cell size with central metabolism. PLoS Genet. *9*, e1003663.

50. Wu, L.J., and Errington, J. (2011). Nucleoid occlusion and bacterial cell division. Nat. Rev. Microbiol. *10*, 8–12.

51. Fernández-Coll, L., Maciag-Dorszynska, M., Tailor, K., Vadia, S., Levin, P.A., Szalewska-Palasz, A., and Cashel, M. (2020). The Absence of (p)ppGpp Renders Initiation of Escherichia coli Chromosomal DNA Synthesis Independent of Growth Rates. MBio *11*, e03223-19.

52. Jin, D.J., and Cabrera, J.E. (2006). Coupling the distribution of RNA polymerase to global gene regulation and the dynamic structure of the bacterial nucleoid in Escherichia coli. J. Struct. Biol. *156*, 284–291.

53. Hadizadeh Yazdi, N., Guet, C.C., Johnson, R.C., and Marko, J.F. (2012). Variation of the folding and dynamics of the Escherichia coli chromosome with growth conditions. Mol. Microbiol. *86*, 1318–1333.

54. Lee, T.S., Krupa, R.A., Zhang, F., Hajimorad, M., Holtz, W.J., Prasad, N., Lee, S.K., and Keasling, J.D. (2011). BglBrick vectors and datasheets: A synthetic biology platform for gene expression. J. Biol. Eng. *5*, 12.

55. Neidhardt, F.C., Bloch, P.L., and Smith, D.F. (1974). Culture medium for enterobacteria. J. Bacteriol. *119*, 736–747.

STAR★METHODS

KEY RESOURCES TABLE

REAGENT or RESOURCE	SOURCE	IDENTIFIER
Bacterial and virus strains		
ppGpp0	Michael Cashel Lab	Strain ID: CF10237
ΔrelA	Michael Cashel Lab	Strain ID: CF12510
NCM3722	Yale Depository	Strain ID: CGSC# 12355
Chemicals, peptides, and recombinant proteins		
IPTG (Isopropyl β- D-1-thiogalactopyranoside)	Sigma-Aldrich	Cat.#I6758-5G
Doxycycline (hyclate)	Sanbio	Cat.#14422-1
Ammonium acetate	Biosolve	Cat.#0001244146BS
Acetic acid	Biosolve	Cat.#0001074131BS
Acetonitrile	Biosolve	Cat.#0001204102BS
Methanol absolute	Biosolve	Cat.#0013684102BS
Trehalose	Sigma-Aldrich	Cat.#27001-500ml
Ammonium hydroxide	Honeywell	Cat.#221228-100ml
Formic acid	Sigma-Aldrich	Cat.#27001-500ml-R
ppGpp (14-N chemical standard)	Trilink	Cat.#N-6001-5
Casamino acids	Sigma-Aldrich	Cat.#82514-1kg
L-Tryptophan	Alpha Aesar	Cat.#J62508
L-Serine	Alpha Aesar	Cat.#J62187
Ammonium chloride 15-N	CORTECNET	Cat.#CN80P10
Tween-20	Bio-Rad	Cat.#1706531
EDTA	Sigma-Aldrich	Cat.#E6758
SDS	Sigma-Aldrich	Cat.#L3771
Critical commercial assays		
PDMS (SYLGARD™) 184 Silicone Elastomere Kit	Farnell	Cat.#01673921
Quant-It RNA HS	Thermo Fisher	Cat.#Q32884
Bradford Reagent Kit	Bio-Rad	Cat.#500-0006
1 mL/30 mg Oasis Wax cartridge	Waters	Cat.#186002489
Durapore Membrane Filter, PVDF, 25mm	Merck Millipore	Cat.#HVLP02500
Deposited data		
Data published in this work	10.5281/zenodo.5602437	N/A
Oligonucleotides		
RelA'_F (AAAAGATCTAGGAGGAAAAAAATGGTTGCGGTAAGAAGTGC)	IDT	N/A
RelA'_R (TTACTCGAGTTAGGATCCCAGCTGGTAGGTGAACGGC)	IDT	N/A
Mesh1_F (AAAAGATCTAGGAGGAAAAAAATG)	IDT	N/A
Mesh1_R (TTTCTCGAGTTAGGATCCCAG)	IDT	N/A
CFP_F (AAAAGATCTAGGAGGAAAAAAATGAGCAAGGGCGAGG)	IDT	N/A
CFP_R (AAACTCGAGTTAGGATCCTTATTTATACAGCTCATCCATGCC)	IDT	N/A
YFP_F (AAAAGATCTAGGAGGAAAAAAATGGTGAGCAAGGGCG)	IDT	N/A
YFP_R (AAATTACTCGAGTTAGGATCCTTACTTGTACAGCTCGTCCATG)	IDT	N/A
Recombinant DNA		
p*relA**	This study	AddGene ID: 175590
p*mesh1**	This study	AddGene ID: 175591
p*YFP*	This study	AddGene ID: 175592

(*Continued on next page*)

Continued

REAGENT or RESOURCE	SOURCE	IDENTIFIER
p*CFP*	This study	AddGene ID: 175593
p*mesh1*	This study	AddGene ID: 175594
p*relA'*	This study	AddGene ID: 175595
Software and algorithms		
Metamorph 7.8.0.0	Molecular Devices	N/A
MATLAB R2020a	MathWorks	N/A
Custom MATLAB Measurement	Tans Lab[34]	N/A
Custom MATLAB Analysis and Plotting	10.5281/zenodo.5602437	N/A
MassHunter 7.0	Agilent	N/A
Other		
SeQuant ZIC-cHILIC 3um, 100Å, PEEK coated HPLC column, 100mm x 2.1mm	Merck Sigma	Cat.#1506570001
SeQuant ZIC-cHILIC Guard, PEEK coated guard column, 20mm x 2.1mm	Merck Sigma	Cat.#150436
Durapore Membrane Filter, PVDF, 25mm	Merck Millipore	Cat.#HVLP02500
1 mL/30 mg Oasis Wax cartridge	Waters	Cat.#186002489
BglII Fast Digest	Thermo Fisher	Cat.#10354330
XhoI Fast Digest	Thermo Fisher	Cat.#10880041
BamHI Fast Digest	Thermo Fisher	Cat.#10334480

RESOURCE AVAILABILITY

Lead contact

Further information and requests for resources, data and materials should be directed to and will be fulfilled by the lead contact, Sander Tans: s.tans@amolf.nl

Materials availability

Plasmids generated and used in this study have been deposited to Addgene. See Key Resources Table (KRT) for catalog numbers.

Data and code availability

Accession numbers are listed in the key resources table. The DOI is listed in the key resources table. Measured data reported in this paper will be shared by the lead contact upon request. Custom MATLAB software (See KRT) used to analyze the data has been made public on GitHub (10.5281/zenodo.5602437). Any additional information required to reanalyze the data reported in this paper is available from the lead contact upon request.

EXPERIMENTAL MODEL AND SUBJECT DETAILS

Strains and plasmids

E. coli strains NCM3722 (CGSC# 12355), *ΔrelA* (CF12510) and ppGpp^0 (CF10237) which were transformed with a combination of *relA'-YFP* (*relA**), *YFP*, *mesh1-CFP* (*mesh1**) or *CFP* induction plasmids were used in all the experiments as described in the figures. Plasmid p*relA** (Addgene Plasmid #175590) was constructed by first replacing *mCherry* on a pBbS2k-RFP plasmid (kanamycin resistance, Tet promoter, sc101** origin) with a DNA sequence encoding the first 455 amino acids of the native *relA* gene (*relA'*). *relA'* was cloned from genomic DNA using primers RelA'_F and RelA'_R which encode restriction sites for BIgBrick[54] integration (BamHI, XhoI and BglII) and a custom RBS (AGGAGGAAAAAA). Lastly *YFP* fluorophore *mVenus* was fused to *relA'* via a glycine-serine linker using restriction cloning to construct p*relA**. *mVenus* was cloned from the Addgene plasmid #26598 using primers YFP_F and YFP_R similarly as p*relA'*.

Codon optimized sequence of *mesh1* (cloned via Mesh1_F and Mesh1_R primers) or *CFP* (cloned via CFP_F and CFP_R primers, from Addgene Plasmid #26598) replaced *mCherry* in the plasmid pBbA5a-RFP (ampicillin resistance, lacUV5 promoter, p15A origin) leading to p*mesh1* (Addgene Plasmid #175594) and p*CFP* (Addgene Plasmid #175593). p*mesh1** (Addgene Plasmid #175591) was built similarly to p*relA** using restriction cloning to fuse *CFP* with *mesh1* via a glycine-serine linker.

All of the induction experiments in this manuscript were done using the fluorescence labeled p*relA** and p*mesh1** plasmids or the negative control plasmids containing only the fluorescence genes *YFP* and *CFP* respectively.

Culture conditions

Chemocompotent NCM3722 cells which were transformed with the p*relA** or p*YFP* plasmids were spread on LB Agar plates with 25 ug/mL kanamycin. p*mesh1** and p*CFP* plasmids were transformed and plated on LB Agar plates with 50 ug/mL ampicillin. Plates older than 3 weeks were discarded and fresh transformations were prepared to prevent possible mutants.

Chemocompotent ppGpp^0 cells were co-transformed with p*relA** and p*mesh1** and plated on LB Agar plates with 50 μg/mL ampicillin, 25 μg/mL kanamycin and 100 μM IPTG to allow growth. Without 100 μM IPTG, leakage from p*relA** inhibits growth enough to prevent visible colonies next day morning (data not shown). Plates with colonies were only used on the day where the colonies first appear (next morning after transformation) as older plates loose viability rapidly.

Cells for bulk and microscopy experiments were grown using defined minimal or rich MOPS medium containing 0.2% (with volume) carbon source (glucose, glycerol or malate) supplemented with 100 μM $MnCl_2$, as described in Lee et al.[55] (See resource table for reagents list). Except Figure S1B, all of the experiments were conducted with glucose as the carbon source. Rich medium is the same as minimal media except for the supplementation of 0.2% Casamino acids, 400 μg/mL serine and 40 μg/mL tryptophan. 50 μg/mL ampicillin and 25 μg/mL kanamycin were added to the media along with appropriate plasmid bearing strains.

For ppGpp sampling experiments, cells were grown as described in Noga et al.[35] Briefly cultures were inoculated from overnights into 250 mL Erlenmeyer flasks containing 25ml fresh media. Flasks were placed in a heated water bath set to 37°C and mixed with a magnetic stirrer. MOPS glucose minimal media containing isotopically labeled $^{15}NH_4Cl$ was used in order to distinguish cellular ppGpp from unlabeled internal standard.

For the microscopy experiments, cells were initially inoculated in a 10 mL tube with 5 mL MOPS rich medium from a single colony in the morning. The tube was placed in a 37°C room on an orbital shaker until the growth becomes visible (OD » 0.1). Cells were then spun down at 4000 G for 5 min and re-inoculated in 10 μL top media. 2 μL of the concentrated cells were injected into the microfluidic chip by hand via a p2.5 pipette. The chip is then placed under the objective in a warm chamber set to 37°C for all the experiments. After cells populate the growth chamber input and output tubes are connected to the chip and appropriate media is pushed through at 500 μl/h. This corresponds to 250-500x dilution per h since the chip's inner volume is between 1-2 μL. The cells were allowed to grow in the chips for 12 h uninterrupted before the experiments start to guarantee steady state growth.

ppGpp^0 strain requires different handling due to its inability to respond to stress. For the 96 well plate experiments, a single colony was inoculated in 5 mL glucose rich media with 100 μM IPTG and placed on a shaker for up to 4 h until OD_{600} reaches 0.4. After that 40 ng/mL dox is added to prime the culture with high ppGpp production which allows it to handle stress and initiate growth in minimal media. This culture is then diluted in fresh media (MOPS minimal with different carbon sources) without any inducers. Immediately after the dilution, 98 μL of the culture is pipetted into wells of 96 well plates together with 1 μL dox and 1 μL IPTG (both at 100x final concentration), reaching a final volume of 100 μL. 96 well plates which were prepared as above were placed in a BioTek Synergy HTX plate reader maintained at 37°C with constant orbital shaking. OD was measured every 10 min.

A similar method is applied for the microscopy experiments with the ppGpp^0 strain. A single colony is grown in rich media with proper antibiotics from the morning and when OD reached 0.1, 40 ng/mL dox is added to induce ppGpp production, which promotes cell survival during chip loading.

METHOD DETAILS

Sample collection and analysis for ppGpp, protein, and RNA quantification

Bulk cultures were induced with IPTG or dox at OD ~0.1 (early exponential phase). Two biological replicates and three sampling replicates from each were used. Samples were taken either at OD ~0.4 (mid exponential phase) for growing cultures or 2.5 h after maximum induction of *relA** (10 ng/mL). Rapid sample quenching, processing, and LCMS-based quantification of ppGpp were performed largely as in Noge et. al.[35] Briefly, 2 mL sample from cultures grown in MOPS medium with $^{15}NH4Cl$ as the sole nitrogen source was pipetted directly onto a prewetted 2.5-cm-diameter 0.45 μm pore-size HV Durapore membrane filter. After vacuum collection, the filter was immediately quenched in 1 ml of ice-cold 2 M formic acid spiked with 10 μl internal standard (IS) ^{14}N-ppGpp. The quenched cell suspension was neutralized with 25 μl of 28% ammonium hydroxide. All samples were stored in −80°C for further processing and measurement.

In order to measure RNA and protein concentrations, first cells lysates were obtained as described in Potrykus et al.[18] Equivalent OD*ml cultures were sampled into 15 mL falcon tubes on ice. The cultures were centrifuged at 4000G for 10 min at 4°C, the pellets were washed with 1 mL 0.9% NaCl solution by resuspending and centrifuging twice at the same setting. 800 μL of suspension after the final wash was lysed in 200 μL EDTA and SDS solution at 95°C for 15 s. Tubes of lysates were then cooled on ice for up to 5 min and stored in −20°C until measurement. Induction and sampling OD's were the same as in ppGpp sampling experiments. Concentration of RNA in the sampled lysates were measured using Quant-It RNA Kit and provided standard samples following manufacturers protocol. Protein concentrations were measured using Bradford Kit reagent from Bio-Rad and standard bovine gamma-globulin samples following manufacturers protocol. For both methods the fluorescence and absorbance measurements were conducted by a BioTek Synergy HTX plate reader using filters 620 (9) nm / 680(20) nm (ex/em) for Quant-It RNA fluorescence or 595nm absorbance for Bradford protein quantification.

Microfluidic flow cell

The microfluidic chip's Epoxy mold which was kindly sent by Daan J. Kiviet from Ackermann Lab is a variant of the mothermachine from Jun lab. Each flow line consists of an input which splits up into 2 arms, in each arm there are a number of extruding growth chambers varying in depth and width (80, 60, 40, 20, 10, 5 μm width, 60, 30, 50, 40 μm depth) and a single output after the 2 arms reconnect into a single line.

Chips were built by first preparing the PDMS mix.[34] Polymer and curing agent (Sylgard 184 elastomer, Dow Corning) were prepared by mixing 7.7 g of polymer with 1mL of curing agent. The slight deviation from the suggested 10 g per 1 mL was implemented to create a more rigid chip allowing low height growth chambers to remain intact. Mixture was then thoroughly mixed using a vortexer and a plastic mixer. Then the mix was poured into the Epoxy mold (provided by Ackermann lab) and placed in a desiccator for 30 min to remove air bubbles formed during mixing. Then the mold is baked at 80°C for 1 h. After the baking period, the PDMS chip was removed from the mold using scalpels and rough edges were cut to allow for better binding to glass. Inlet and outlet holes were punched using a hole puncher. The PDMS chip was then covalently attached to a glass slide by using a hand-held corona treatment device (model BD-20ACV, Electro-Technic Products). Application was done by passing the corona treatment device 6-7 times, each pass lasting ~5 s, 5-10 mm away from the surface of both the PDMS chip and glass coverslip. After the corona application, PDMS chips were placed on the treated glass surface and tapped by a gloved finger to assure full bonding. Prepared chips could be used for some weeks after preparation however after more than a month, chambers start to collapse, therefore chips older than 1 month were not often used.

Imaging and image analysis

Cells growing in the microfluidic chambers were imaged using an inverted Nikon TE2000. Using 100x and a 1.5x zoom lenses in tandem a pixel size of 0.041 μm was achieved. Imaging was done using a CMOS camera (Hamamatsu Orca Flash 4.0) via illumination from an LED light source (ImSpec, HPX-L5) with a liquid light guide. The microscope stance was equipped with a computer-controlled stage (Marzhauser, SCAN IM 120 3 100) allowing the stage to move between several chambers for imaging. A phase contrast image was taken every minute and a fluorescence image every 5 min using Chroma filter set 49003 and a computer-controlled shutter (Sutter, Lambda 10-3 with SmartShutter). Control of the automated microscopy systems was achieved through MetaMorph software. Each experiment lasts between 24-36 h.

Images were initially visually checked for issues such as cells washing away from the wells or halting of growth due to clogs. After the initial checks, a MATLAB based software customized by the Tans Lab was used to quantify growth rates, cell volumes and fluorescence. Individual cells were identified and tracked from phase contrast images. Cell's lengths and volumes were estimated assuming the shape of cylinders with semicircular caps and fitting a polynomial to skeletons of binary cell masks. Estimated length data through time was used to calculate instantaneous growth rate and average growth rate using exponential fits. Fluorescence values were calculated from a strip inside the cell area to decrease errors caused by fluorescence falloff that occurs at the edges of the cell. Added length was calculated by subtracting length at division (end of cycle) from length at birth (beginning of cycle). Duration of the cycles were calculated as the time between birth and division. Width was calculated from the fitted cylinder. Any cell that did not divide within the growth chamber was ignored since complete cell cycles are needed to analyze division phenomena. Cells that approached the exits of the wells were also eliminated from the analysis due to tracking issues caused by increased cell speeds near the exit.

ppGpp quantification via LC/MS

All LC/MS runs were performed using a Agilent LC/MS system consisting of a binary pump (G1312B), an autosampler (G7167A), a temperature-controlled column compartment (G1316A), and a triple-quadrupole (QQQ) mass spectrometer (G6460C) equipped with a standard electrospray ionization (ESI) source, all operated using MassHunter data acquisition software (version 7.0).

Samples stored in −80°C were defrosted by 1 to 2 min of incubation in a 37°C water bath and sonicated for 10 min in a water-ice slurry. After 10 min of centrifugation at 20,000 × g, samples were loaded on a 1 mL/30 mg Oasis Wax cartridge (Waters) preconditioned with 1 ml of MeOH and 1 ml 50 mM ammonium acetate buffer (pH 4.5). After washing with 1 ml ammonium acetate buffer and MeOH was performed, cartridges were left under vacuum for 1-2 min for excess MeOH to evaporate before eluting the ppGpp with 200 μl of 2.8% ammonium hydroxide–MeOH/ACN/H2O 50:30:20 (vol/vol/vol). After addition of 10 μl of 5% trehalose and brief vortex mixing, the samples were dried in a vacuum centrifuge (Labconco). Dried trehalose-stabilized extracts were redissolved in 20 μl of MeOH/ACN/H2O (50:30:20 [vol/vol/vol]) and moved to an autosampler vial for analysis. Separation was performed on an iHilic column (Hilicon) (2.1 mm by 100 mm, 3.5-μm pore size) or a SeQuant Zic-cHILIC column (Merck) (2.1 mm by 100 mm, 3-μm pore size) at 0.3 mL/min using the following binary gradient: 100% B, ramp to 85% B in 1.5 min followed by 10 min of isocratic hold at 85% B and a linear decrease to 30% B in 3 min with a 2-min hold at 30% B and 8 min reequilibration under the initial conditions (A, 3.75 mM ammonium acetate–1.25 mM acetic acid–2 mM acetylacetone–Milli-Q water, B, 11.25 mM ammonium acetate–3.75 mM acetic acid–2 mM acetylacetone–80% ACN). The injection volume was 2 μl.

Peak areas measured for the internal standards (unlabeled) were used to correct the peak areas of biological ppGpp (labeled) assuming relative sample loss to be equal between the two during the multi day sampling and processing steps.

QUANTIFICATION AND STATISTICAL ANALYSIS

Sample numbers corresponding to the statistical tests are described in figure legends and in the results section. Two-sample t test were used ($p < 0.05$) when comparing samples represented in boxplots. Boxplots depict median (central mark), 25 and 75 percentile (boxes) and extremes (whiskers) of the represented data. Error bars on binned averages represent standard deviation.

Calculation of response time

For Figure 2E, data points within a sliding window of width $\sim T_{cyc}$ were compared against the data points where growth rate became stable after induction for each experiment. As the sliding window moves through time (1 min steps), both growth rate and added length change and approach the final stable value. When the t test between the data points in the sliding window and in the final stable growth regime yielded a p value that exceeded 0.05 in three consecutive sliding time steps, the center of the window was defined as the "stabilization time." For each experiment the data was randomly split into 3 parts and each part was analyzed using the same method (black dots, Figure 2D). Cells were ordered according to their division time and placed into the 3 different groups. Since in each frame there are multiple divisions, this method keeps the data density through time similar between the 3 random subsamples.

Division frequency analysis

Boxplots (Figures 3D–3F) were determined for measured values of $60/T_{cyc}$, in a period between 150 min. before induction and the moment of induction (green), and in a period between the moment of induction until two times the average pre-shift cell cycle time (blue).

Double normalization

In order to visually compare the changing rates of growth, division and cell size; a 2-sided normalization method was used. For each quantity, initial and final values were arbitrarily normalized to 2 and 1 respectively. Values of a and b were calculated such that [BeforeShiftAverage]*a+b = 2 and [AfterShiftAverage]*a+b = 1 from here the entire set of datapoints were normalized by [DataNorm.] = [Data]*a+b. This leads to vertical scaling of the data and allows visual comparison of different datasets with different start and end values. Since 2 and 1 were arbitrarily selected, when plotting, 'Initial' and 'Final' were chosen as labels for clarity.

Models

We considered two alternative models describing size control during the transient. In both models a cell divides with a hazard rate[36] that depends on the added size and a target added size ΔL (which in stationary conditions corresponds to the average added size). Both the target added size $\Delta L(t)$ and the growth rate $\mu(t)$ are functions of time during the transient. In both the models the growth rate $\mu(t)$ is exponentially relaxing to the stationary value observed in each of the experiments. The two models differ for the relation between growth rate and size scale during transient. In the hierarchical model, the typical size is a deterministic function of the growth rate ($\Delta L(t) = D*\exp(\mu(t)*T)$. Parameters were as follows: $T = \log(\Delta L\text{Final}/\Delta L\text{Initial})/(\mu\text{Final} - \mu\text{Initial})$ and $D = \Delta L\text{Initial}*\exp(-\mu\text{Initial}*T)$. In the direct model, $\Delta L(t)$ is relaxing to the stationary value linearly in two pre-shift cycle duration time. A more detailed description of both models can be found in Methods S1.